Biomaterials 34 (2013) 4118–4127

Contents lists available at SciVerse ScienceDirect

Biomaterials

journal homepage: www.elsevier.com/locate/biomaterials

Imaging specificity of MR-optical imaging agents following the masking of surface charge by poly(ethylene glycol)

Shou-Cheng Wu [a], Kun-Liang Lin [a], Tzu-Pin Wang [b], Shey-Cherng Tzou [a], Gyan Singh [a], Ming-Hung Chen [a], Tian-Lu Cheng [c], Chiao-Yun Chen [d], Gin-Chung Liu [d], Te-Wei Lee [e], Shao-Hwa Hu [f], Yun-Ming Wang [a,*]

[a] Department of Biological Science and Technology, Institute of Molecular Medicine and Bioengineering, National Chiao Tung University, No. 75 Bo-Ai Street, Hsinchu 300, Taiwan
[b] Department of Medicinal and Applied Chemistry, Kaohsiung Medical University, Kaohsiung 807, Taiwan
[c] Department of Biomedical Science and Environmental Biology, Kaohsiung Medical University, Kaohsiung 807, Taiwan
[d] Department of Medical Imaging, Kaohsiung Medical University Hospital, Kaohsiung 807, Taiwan
[e] Isotope Application Division, Institute of Nuclear Energy Research, Lungtan, Taoyuan 325, Taiwan
[f] Chemical Systems Research Division, Chung Shan Institute of Science and Technology, Lungtan, Taoyuan 325, Taiwan

ARTICLE INFO

Article history:
Received 22 January 2013
Accepted 10 February 2013
Available online 1 March 2013

Keywords:
EGFR
Erbitux
MnMEIO
MRI
Nanocarrier

ABSTRACT

The coupling of specific antibodies to imaging agents often improves imaging specificity. However, free amine groups designed for the coupling can cause nonspecific binding of the imaging agents. We report here development of a nanocarrier, MnMEIO-silane-NH_2-mPEG nanoparticles (NPs), consisting of a manganese-doped iron oxide nanoparticle core (MnMEIO), a copolymer shell of silane and amine-functionalized poly(ethylene glycol) (silane-EA-mPEG). The key feature in MnMEIO-silane-NH_2-mPEG is the flexible PEG, which masks the non-conjugated reactive amine groups ($-NH_2 \leftrightarrow -NH_3^+$) and reduces nonspecific binding of MnMEIO-silane-NH_2-mPEG to cells. The amine groups on MnMEIO-silane-NH_2-mPEG were conjugated with the fluorescent dye, Cy777 or antibodies [Erbitux (Erb)] to form a MR-optical imaging contrast agent (MnMEIO-silane-NH_2-(Erb)-mPEG) for EGFR-expressing tumors. Confocal microscopic and flow cytometric analyses showed that MnMEIO-silane-NH_2-(Erb)-mPEG displayed low nonspecific binding. Moreover, TEM images showed that MnMEIO-silane-NH_2-(Erb)-mPEG were endocytosed by EGFR-expressing cells. In line with their EGFR expression levels, A431, PC-3, and Colo-205 tumors treated with MnMEIO-silane-NH_2-(Erb)-mPEG NPs showed −97.1%, −49.7%, and −2.8% contrast enhancement, respectively, in *in vitro* T_2-weighted MR imaging. *In vivo* T_2-weighted MR imaging and optical images showed that MnMEIO-silane-NH_2-(Erb)-mPEG could specifically and effectively target to EGFR-expressing tumors in nude mice; the relative contrast enhancements were 7.94 (at 2 h) and 7.59 (at 24 h) fold higher in A431 tumors as compared to the EGFR-negative Colo-205 tumors. On the contrary, MnMEIO-silane-NH_2-(Erb) NPs showed only 1.44 (at 2 h) and 1.52 (at 24 h) fold higher in EGFR-positive tumors as compared to the EGFR-negative tumors. Finally, antibodies can be readily changed to allow imaging of other tumors bearing different antigens. These data indicate that masking surface charges on contrast agents is a useful strategy to improve imaging efficacy.

1. Introduction

Recently, there has been a considerable interest in developing targeted dual-modality MR-optical imaging agents for early cancer detection [1,2]. The development of these imaging agents often requires conjugation of tumor-targeting moieties and near infrared (NIR) molecules onto the surface of superparamagnetic iron oxide (SPIO) nanoparticles (NPs) [3–6]. The surface modification of NPs with linear chains of poly(ethylene glycol) (PEG) derivatives possessing terminal functional groups such as amine or carboxylic acid is the most common strategy employed for conjugation [7–10].

However, non-conjugated reactive functional groups on the surface of NPs can cause severe fouling and nonspecific interaction of NPs to the cell membranes and may lead to inefficient tagging of NPs to the desired targets and ambiguous detection of unintended targets [11–13]. These inadequacies can severely jeopardize the usefulness of the imaging modality. Consequently, intelligent designs of surface structure that achieve excellent stability, multifunctionality and high targeting specificity are urgently needed [14,15]. Previous studies have demonstrated that neutral and

* Corresponding author. Tel.: +886 3 5712121x56972; fax: +886 3 5729288.
E-mail address: ymwang@mail.nctu.edu.tw (Y.-M. Wang).

0142-9612/$ – see front matter © 2013 Elsevier Ltd. All rights reserved.
http://dx.doi.org/10.1016/j.biomaterials.2013.02.025

negatively charged NPs adhere much less to the negatively charged cell membranes than the positively charged NPs [16–18]. Therefore, there have been constant efforts to neutralize the surface charge. Recently, surface modification of NPs by zwitterionic ligands has been successfully used to achieve neutral surface [17–19], however, the approaches requires multi-step processing of the NPs.

In this study, we aim to develop a base system for targeted contrast agents that display low nonspecific binding while targeting antibodies are easily replaceable. The design is based on the flexibility of poly(ethylene glycol) which could in principle covers non-conjugated functional group to prevent nonspecific binding of the contrast agents. This approach could be used as a model system to investigate the benefits of masking surface charges on improving the specificity of NPs. The molecular structure of silane-EA-mPEG was strategically designed and synthesized (Scheme 1) such that the non-conjugated $-NH_2$ ($-NH_2 \leftrightarrow -NH_3^+$) on the surfaces of NPs remain buried deep inside the entangled mPEG chains as shown in Fig. 1. Thus, mPEG can act as an insulator, which in turn can decrease the electrostatic interaction between NPs and negatively charged cell membranes of non-targeted tissue. Thus, these two NPs were expected to display different surface charges.

In addition, we aimed to develop a dual-modality MR-optical imaging contrast agent, which could be used to image *in vitro* and *in vivo* tumors by both MR and optical imaging techniques. To this aim, we synthesized superparamagnetic iron oxide nanoparticles, MnMEIO-silane-NH_2-(Erb)-mPEG NPs, containing the linear chains of poly(ethylene glycol) (PEG), near infrared fluorescence dye (Cy777), and Erbitux (Erb, an EGFR targeting monoclonal antibody). The binding ability of the contrast agents to EGFR-expressing tumors (A431, SKBR-3, PC-3, and Colo-205) [20] was evaluated by flow cytometric analysis, confocal fluorescent microscopy, and *in vitro* T_2-weighted MR imaging. Moreover, the binding specificity of MnMEIO-silane-NH_2-(Erb)-mPEG NPs were investigated and compared to other imaging agents by flow cytometry and confocal microscopy. Finally, nude mice bearing subcutaneous xenografts of A431 and Colo-205 tumors were used for MR and optical imaging to test the usefulness of MnMEIO-silane-NH_2-(Erb)-mPEG for *in vivo* imaging.

2. Experimental

2.1. Chemicals

Osmium tetroxide (1%), iron (III) acetylacetonate (Fe(acac)3, 99.9%), manganese (II) chloride ($MnCl_2 \cdot 4H_2O$, 99%), methyl poly(ethylene glycol) (mPEG, M.W. = 2000), oleic acid (90%), oleylamine (90%), *N*-ethyl-*N*′-(3-dimethylaminopropyl) carbodiimide (EDC), IR-783, Fluorescein isothiocyanate (FITC), and glutaraldehyde (25%) were purchased from Sigma–Aldrich (St. Louis, MO, USA). Acryloyl chloride (96%) and *N*-Boc-ethylenediamine (98%) were purchased from Alfa Aesar (Ward Hill, MA, USA). (3-Aminopropyl) triethoxy silane (APTES, 98%) was purchased from Fluka (Buchs, Switzerland). Cetuximab (Erbitux) was purchased from Merck (Dietikon, Switzerland). (Benzotriazol-1-yloxy) tripyrrolidinophosphonium hexafluorophosphate (PyBOP) and *N*-hydroxybenzotriazole (HOBt) were purchased from NovaBiochem (Nottingham, UK). BCA (bicinchoninic acid) protein assay reagent kit was purchased from Pierce (Rockford, IL, USA). Molecular-porous membrane tubing (M.W. = 12–14 kDa and M.W. = 50 kDa) was purchased from Spectrum (Houston, TX, USA). S162 Scientific Formvar/Carbon 200-mesh copper (50-grid) was purchased from Agar Scientific (Stansted, UK). Matrigel was purchased from BD Bioscience (Bedford, MA, USA). Spurr's resin was purchased from Agar Scientific (Stansted, Essex, UK). All chemicals were used directly without any further purification unless otherwise stated. The details of the synthesis of mPEG-AC, APTES-Ac, silane-N-Boc-EA-mPEG, silane-EA-mPEG, Cy777, MnMEIO-silane-NH_2-mPEG, MnMEIO-silane-NH_2-(Erb or Her)-mPEG, MnMEIO-silane-NH_2, and MnMEIO-silane-NH_2-(Erb or Her) NPs are reported in Supporting Information.

2.2. Characterization

Relaxation time values (T_1 and T_2) of aqueous solutions of MnMEIO-silane-NH_2-(Erb)-mPEG NPs were measured to determine relaxivity r_1 and r_2. All measurements were made using a relaxometer operating at 20 MHz and 37.0 ± 0.1 °C (NMS-120 Minispec, Bruker, Ontario, Canada). The ^{1}H NMR (300 MHz) spectra were recorded on a Varian Unity-300 NMR spectrometer (Varian, Palo Alto, CA, USA). The FT-IR analyses were performed using a Fourier transform infrared (FT-IR, Perkin–Elmer, spectrum 2000, Boston, MA, USA). Hydrodynamic size and zeta potential were analyzed with dynamic light-scattering (DLS, Nano ZS90, Malvern Instruments, UK). The EDS spectra of MnMEIO and MnMEIO-silane-NH_2-mPEG NPs were obtained on an Energy-dispersive spectrometer (EDS, S-3000N, Hitachi, Tokyo, Japan). The amount of antibody was determined UV/Vis spectrometry (Hitachi, U-3010, Tokyo, Japan). Magnetic properties of the MnMEIO were studied with superconducting quantum interference devise magnetometer (SQUID, VSM; Model 7400, Lake Shore, Westerville, OH, USA) at fields ranging from −10 to 10 kOe and at 298 K.

2.3. Determination of conjugation efficiency between Erbitux antibodies with NPs

The conjugation efficiency between Erbitux antibodies with MnMEIO-silane-NH_2-mPEG NPs or MnMEIO-silane-NH_2 NPs was determined by collecting

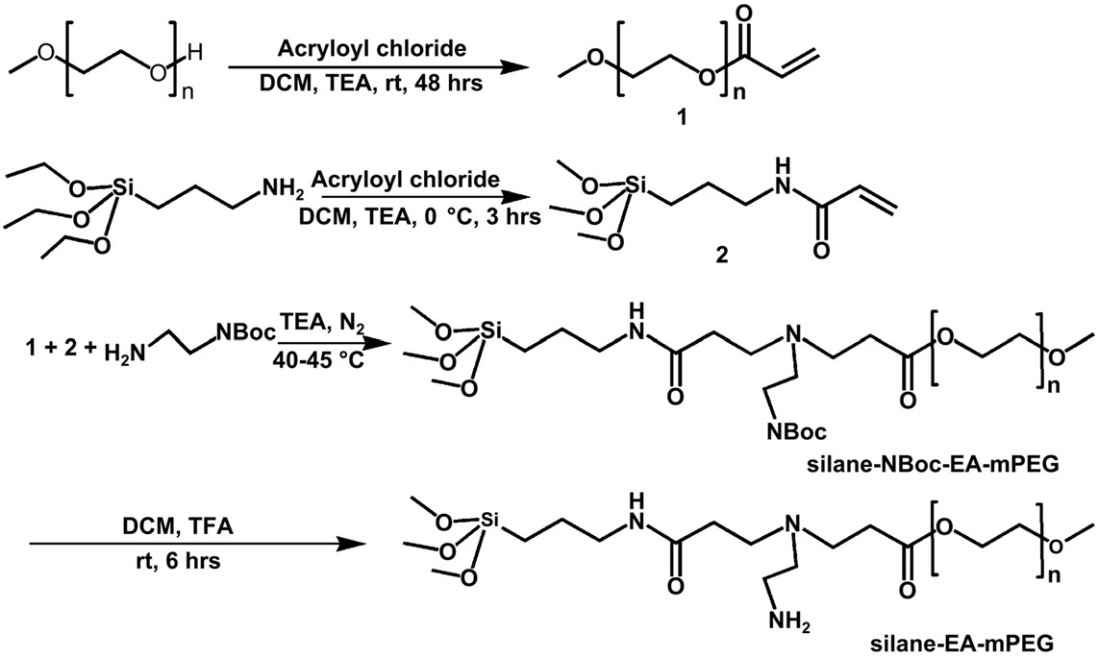

Scheme 1. Synthetic scheme of silane-EA-mPEG.

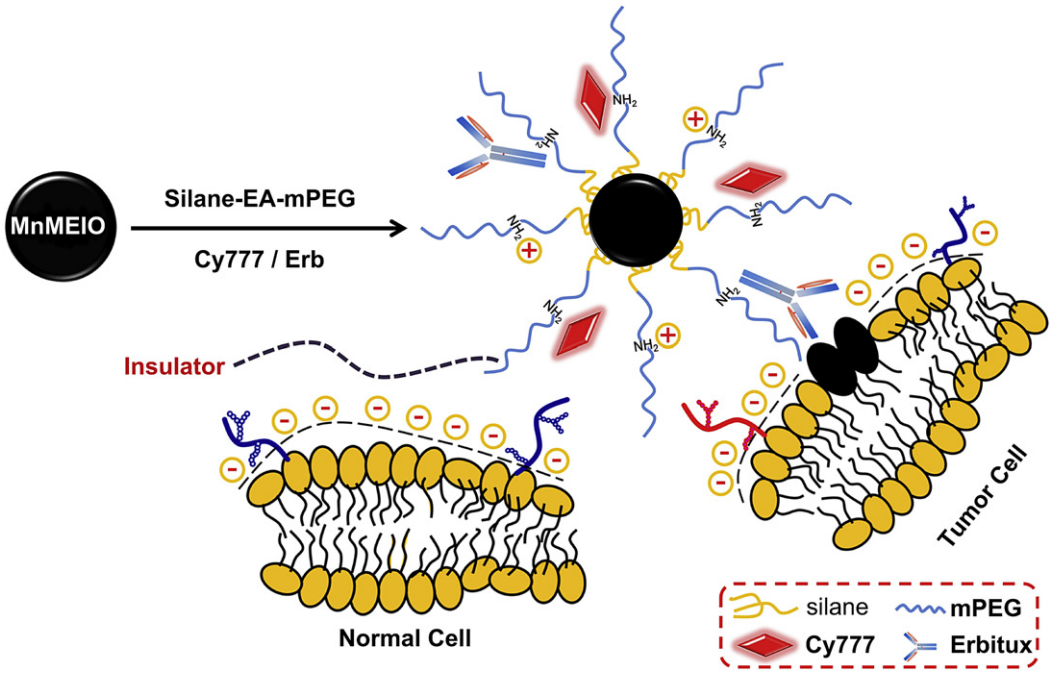

Fig. 1. Schematic illustration of enhancing specific targeting of protonated MnMEIO-silane-NH_2-(Erb)-mPEG NPs by masking positive charges on the NPs.

unconjugated oligonucleotides in the supernatant after centrifugal filtration of the Erbitux antibody reaction mixture and measuring the concentration using NanoDrop ND-1000 Spectrometer (NanoDrop products, Wilmington, DE, USA). These data were presented as mean ± SD calculated from quadruple wells.

2.4. Cell lines and animal model

Epidermal growth factor receptor (EGFR)-expressing cells, A431 (a human epidermoid cancer cell line), SKBR-3 (a human breast cancer cell line), PC-3 (a human prostate cancer cell line), and a low or non EGFR-expressing cell Colo-205 (a human colorectal cancer cell line) were cultured in DMEM, McCoy's 5A medium, DMEM/Hams F12 medium, and RPMI 1640 medium, respectively, supplemented with 10% fetal bovine serum (FBS) (GIBCO). All cells were cultured in a humidified incubator at 37 °C with 5% CO_2.

HER2/neu receptors expressing cells, SKBR-3 (a human breast cancer cell line), MCF-7 (human breast adenocarcinoma cell line), and a low or non HER2/neu-expressing cell Colo-205 (a human colorectal cancer cell line) were cultured in DMEM, McCoy's 5A medium, and RPMI 1640 medium, respectively, supplemented with 10% fetal bovine serum (FBS) (GIBCO). All cells were cultured in a humidified incubator at 37 °C with 5% CO_2.

Female BALB/cAnN.Cg-Foxn1nu/CrlNarl mice (6–8 weeks old) were purchased from the National Laboratory Animal Center, Taipei, Taiwan. Animal experiments were performed in accordance with the institutional guidelines. One million (1×10^6) A431 and Colo-205 cells were subcutaneously injected to right and left flanks, respectively, of nude mice ($n = 3$) in 100 μL PBS with matrigel. MR imaging experiments (see below) were performed two weeks after tumor implantation, at which time the tumors were measured approximately 500 mm^3 in volume.

2.5. Flow cytometric analysis

A431, PC-3, and Colo-205 cells were collected in microcentrifuge tubes (1×10^6 cells each). These cells were incubated with MnMEIO-silane-NH_2-(Erb)-mPEG NPs and control probes (MnMEIO-silane-NH_2-mPEG NPs, MnMEIO-silane-NH_2-(Erb) NPs, and MnMEIO-silane-NH_2 NPs) (10 μg/mL) for 1 h at 37 °C, and the cells were washed three times in PBS, and then resuspended by 1 mL PBS in FACS tube. Immunofluorescence of viable cells was analyzed by a FACScan flow cytometer (Becton Dickinson, San Jose, CA). Fluorescent intensities were analyzed with the CELLQUEST software (Becton Dickinson).

2.6. Confocal fluorescent microscopy

All cell lines (A431, SKBR-3, PC-3, MCF-7, and Colo-205) were seeded at a density of 2×10^5 cells/well on cover glasses (24 × 24 mm) and grown for 24 h. Then cells were incubated with MnMEIO-silane-NH_2-(Erb)-mPEG NPs or MnMEIO-silane-NH_2-(Her)-mPEG NPs and control probes (MnMEIO-silane-NH_2-mPEG NPs, MnMEIO-silane-NH_2-(Erb) NPs or MnMEIO-silane-NH_2-(Her) NPs, and MnMEIO-silane-NH_2 NPs) (10 μg/mL) for 1 h at 37 °C, washed three times in PBS, and fixed with 4% formaldehyde solution for 30 min at room temperature. Cell nuclei and cytoplasm were stained with 4′-6-diamidino-2-phenylindole (DAPI, blue) and HiLyte Fluor™ 594 acid (red), respectively. Cover glasses containing fixed cells were mounted in a mixture of PBS and glycerol (1 : 1) on a microscope slide. The cells were observed using a laser scanning confocal imaging system (Olympus Fluoview 300, Olympus, Tokyo, Japan) consisting of Olympus BX51 microscope (Olympus, Tokyo, Japan) and a 20 mW-output 488 nm argon ion laser.

2.7. TEM measurements

The average core sizes, size distribution, and morphology of the nanoparticles were examined using a transmission electron microscope (TEM, JEOL JEM-2000 EXII, Tokyo, Japan) at a voltage of 100 kV. An aqueous solution of MnMEIO-silane-NH_2-(Erb)-mPEG NPs was drop-casted onto a 200-mesh copper grid and the grid was air-dried at room temperature before TEM measurements.

A431, PC-3, and Colo-205 tumor cells treated with contrast agents were prepared and analyzed by TEM as following: tumor cells (1×10^6 cells) grown on glass coverslips were incubated with MnMEIO-silane-NH_2-(Erb)-mPEG NPs (10 μg/mL) for 24 h. After washed 3 times in PBS to remove unbounded NPs, tumor cells were trypsinized and washed 5 times in PBS and fixed in 2.5% glutaraldehyde for 2 h. Fixed cells were washed 3 times in PBS. Post-fixation staining was done using 1% osmium tetroxide for 1 h at room temperature. Tumor cells were washed and dehydrated in 40, 50, 70, 80, 90, 95, and 100% ethanol successively and treated twice, 30 min each, with propylene oxide, followed by embedding in Spurr's resin. A diamond knife was used to section the embedded cells. The sections were post-stained with 2.5% aqueous uranyl acetate and 0.2% aqueous lead citrate. Prepared cell samples were then analyzed by the transmission electron microscope at a voltage of 100 kV.

2.8. In vitro MR imaging study

MR imaging was performed on a 7.0 T MRI system (Bruker, Ettlingen, Germany). All cell lines (A431, PC-3, and Colo-205 cells) contained 1×10^6 cells, were incubated with MnMEIO-silane-NH_2-(Erb)-mPEG NPs (10 μg/mL) for 1 h at 37 °C and washed three times in PBS. All samples were scanned by a fast gradient echo pulse sequence (TR/TE = 3000/90). The contrast enhancement (%) was calculated by the following equation (Eq. (1))

$$\text{Enhancement}(\%) = (SI_{post} - SI_{pre})/SI_{pre} \times 100 \quad (1)$$

where SI_{post} is the value of signal intensity in tumor cells treated with the contrast agents, MnMEIO-silane-NH_2-(Erb)-mPEG NPs, and SI_{pre} is the value of signal intensity for tumor cells alone.

2.9. In vivo MR imaging study

Nude mice bearing A431 and Colo-205 tumor cells (approximately 500 mm^3) were anesthetized by pentobarbital. MnMEIO-silane-NH_2-(Erb)-mPEG NPs and control probe (MnMEIO-silane-NH_2-mPEG NPs, MnMEIO-silane-NH_2-(Erb) NPs, and MnMEIO-silane-NH_2 NPs) (10 mg/kg) were infused via the tail vein to the mice. The MR imaging was performed on a Bruker 7.0-T Biospec MR scanner (Bruker, Ettlingen, Germany) with a volume coil used as radio frequency (RF) transmitter and receiver. All mice were measured using a T_2-weighted fast spin-echo sequence (TR/TE = 3000/90, echo train length = 8) imaging for every 3 mm sectioning thickness. Images were acquired at pre-injection and various time points (2.0 and 24.0 h) post-injection. The contrast enhancement (%) was calculated by the equation (Eq. (1)), where SI_{post} is the value of signal intensity for contrast agent targeted on tumor cells, and SI_{pre} is the value of signal intensity before contrast agent injection.

2.10. In vivo optical imaging study

Tumor-bearing mice were anesthetized and injected via tail vein with MnMEIO-silane-NH_2-(Erb)-mPEG NPs and control probe (MnMEIO-silane-NH_2-mPEG NPs, MnMEIO-silane-NH_2-(Erb) NPs, and MnMEIO-silane-NH_2 NPs) (10 mg/kg). Optical imaging were acquired at pre-injection and various time points (2.0, and 24.0 h) post-injection using an IVIS spectrum system (IVIS Imaging System 200 Series, Caliper Life Sciences, USA) Images collected were analyzed by Living Image software version 3.0 (Xenogen).

2.11. Histological analysis

Tumor-bearing mice were sacrificed 24 h after MR imaging studies, A431 and Colo-205 tumoral biopsies were fixed in 10% formalin and embedded in paraffin. Tumor blocks were sectioned and stained with H&E. To detect MnMEIO-silane-NH_2-(Erb)-mPEG NPs, sections were stained with Prussian blue against MnMEIO NPs.

3. Results and discussion

3.1. Synthesis of MR-optical imaging agents

The aim of this study was to develop an optimal nanocarrier with minimal nonspecific binding. To this aim, we used a PEG derivative (silane-EA-mPEG) to construct this nanocarrier. This strategically designed and synthesized polymer (Scheme 1) in principle could cover up an amine group inside the entangled mPEG chains (Fig. 1). Therefore, mPEG act as an insulator, which can decrease the electrostatic interaction between NPs and negatively charged cell membranes to reduce nonspecific binding. The synthesis of silane-EA-mPEG was carried out via Michal addition of *N*-Boc-ethylenediamine, methoxypoly (ethylene glycol) acrylate

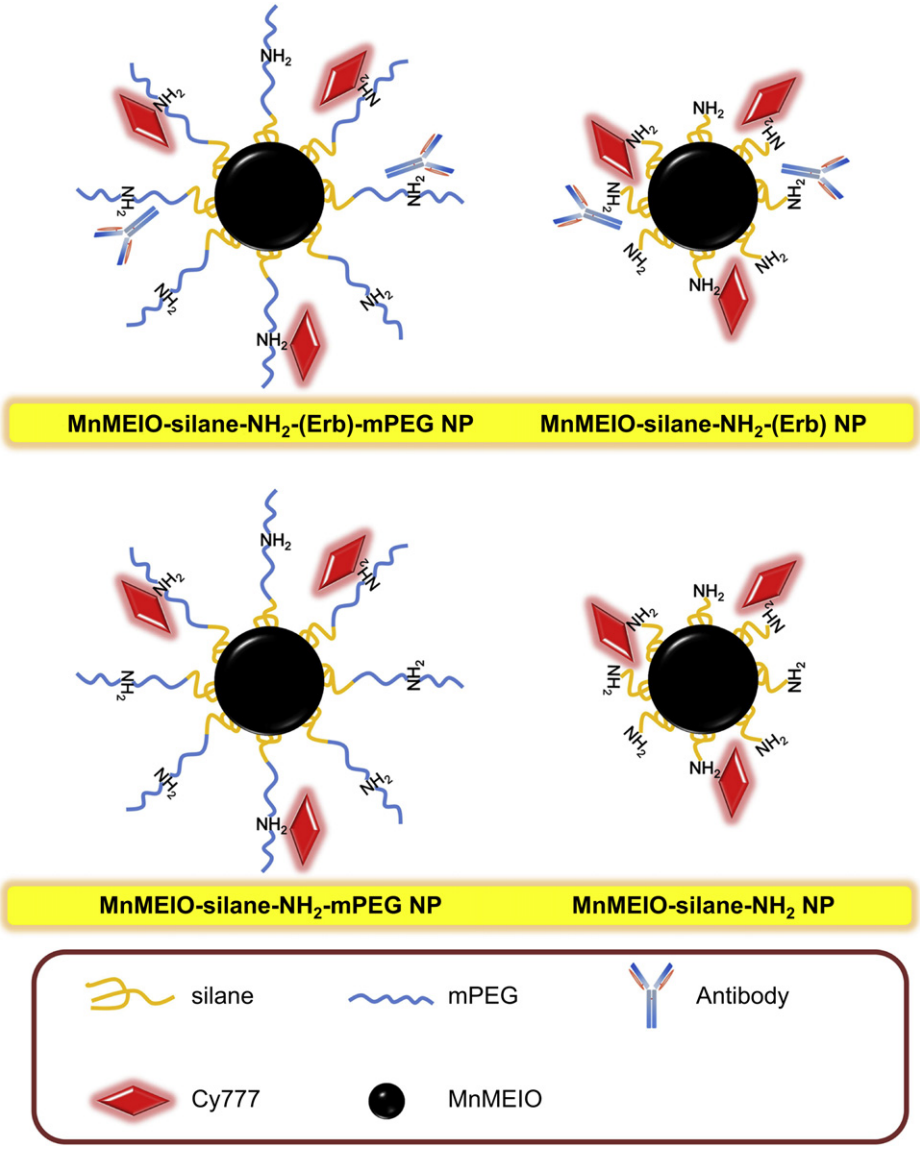

Fig. 2. Schematic representations of the NPs.

(mPEG-Ac) and (3-aminopropyl) triethoxy silane acrylate (APTES-Ac) followed by Boc deprotection. Manganese-doped magnetism-engineered iron oxide (MnMEIO) NPs with an average diameter of 8.8 ± 0.8 nm (Supporting Information, Figure S1) were synthesized using a non-hydrolytic thermal decomposition process. The magnetization curve obtained at room temperature showed no hysteresis (Supporting Information, Figure S2) and the saturation magnetization (Ms) of MnMEIO NPs obtained from the magnetization curve was 101 emu/g. The silane-EA-mPEG coated MnMEIO NPs were prepared using a ligand–exchange reaction between as-prepared oleic acid, oleyl amine-stabilized MnMEIO NPs, and silane-EA-mPEG. Successful ligand exchange was confirmed by Fourier transform infrared spectroscopy (FT-IR) and energy-dispersive spectrometer (EDS) analyses (Supporting Information, Figure S3 and Table S1). In addition, the EDS spectra also show characteristic strong Si peak after ligand exchange (Supporting Information, Figure S4). Dynamic light-scattering (DLS) measurements revealed that silane-EA-mPEG coated MnMEIO NPs have a relatively narrow size distribution with a mean size of 35.1 ± 4.2 nm (Supporting Information, Figure S5). The grafted amine groups served as reactive sites for efficient conjugation of with Cy777 dye and Erb or Her. The carboxylic acid in Cy777 dye was briefly activated with *N*-ethyl-*N*′-(3-dimethylaminopropyl) carbodiimide (EDC) in dimethyl sulfoxide (DMSO) and the activated Cy777 was conjugated to the surface of MnMEIO-silane-NH_2-mPEG NPs. The DLS analyses show that the diameters of Cy777 and Erb conjugated with MnMEIO-silane-NH_2-mPEG NPs increased from 35.1 ± 4.2 to 48.2 ± 5.9 nm (Supporting Information, Figure S5) and the zeta potential value dropped from +17.3 ± 0.7 to +7.1 ± 0.2 mV at pH 7 due to the shielding of amine groups (Supporting Information, Figure S6). Conjugation efficiency of Erb antibodies to the MnMEIO-silane-NH_2-mPEG was 76 g/mg NPs. Therefore, these results confirmed that the Cy777 and Erb were conjugated onto the surface of MnMEIO-silane-NH_2-mPEG NPs. The relaxivities (r_1 and r_2) of the MnMEIO-silane-NH_2-(Erb)-mPEG NPs measured at 20 MHz and 37.0 ± 0.1 °C were 26.7 ± 2.3 and 216.9 ± 10.8 mM^{-1} s^{-1}, respectively (Supporting Information, Figure S7). Furthermore, our DLS data indicate no significant variation in hydrodynamic size of MnMEIO-silane-NH_2-(Erb)-mPEG NPs across a wide pH range (pH 4–10) (Supporting Information, Figure S8), reassuring high colloidal stability of MnMEIO-silane-NH_2-(Erb)-mPEG NPs under physiological conditions. Finally, no significant variation in hydrodynamic size and relaxivity of MnMEIO-silane-NH_2-(Erb)-mPEG NPs were observed over a period of two months (Supporting Information, Figures S9 and S10).

We synthesized contrast agents, MnMEIO-silane-NH_2-(Erb)-mPEG, MnMEIO-silane-NH_2-(Erb), MnMEIO-silane-NH_2-mPEG and MnMEIO-silane-NH_2 that differ in the positions of the positively charged amine groups. The schematic representations of these NPs are shown in Fig. 2. Each NP was coated with APTES, followed by hydration which leads to exposure of amine groups. The APTES-coated iron oxide nanoparticles exhibited a high positive zeta potential value (+45.3 ± 0.3 mV at pH 7) in water (Supporting Information, Figure S11). A comparison of FT-IR spectra for MnMEIO NPs and the MnMEIO-silane-NH_2 before and after ligand exchange are shown in Supporting Information, Figure S12 and Table S2. The average size of the nanocarrier was 21.5 ± 1.3 nm; this value was consistent with DLS measurements (Supporting Information, Figure S13). This high positive charge of the nanocarrier is expected to incur much of nonspecific binding effect. Sizes and zeta potential of the nanoparticles are shown in Supporting Information Table S3. Conjugation efficiency of the Erb antibodies onto MnMEIO-silane-NH_2 was 86 g/mg NPs.

3.2. Flow cytometric analysis

In our design, Erb antibody was conjugated in MnMEIO-silane-NH_2-(Erb)-mPEG NPs and MnMEIO-silane-NH_2-(Erb) NPs whereas MnMEIO-silane-NH_2-mPEG NPs and MnMEIO-silane-NH_2 NPs did not contain this antibody. We tested whether MnMEIO-silane-NH_2-(Erb)-mPEG NPs could efficiently and specifically bind to EGFR-expressing tumors by flow cytometry. Three kinds of cancer cells, A431 (expresses high levels of EGFR), PC-3 (expresses medium levels of EGFR) and Colo-205 (expresses low or none EGFR) were incubated with either MnMEIO-silane-NH_2-(Erb)-mPEG NPs or

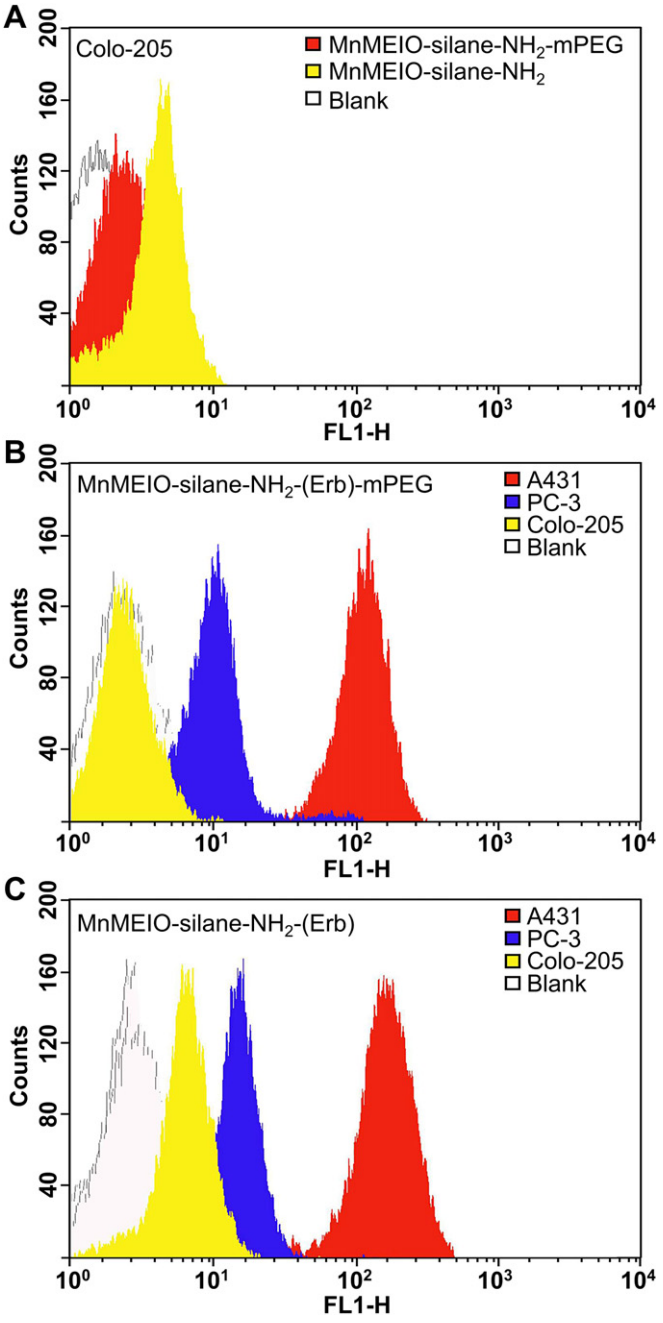

Fig. 3. Binding specificity of the NPs. Comparison of nonspecific binding of MnMEIO-silane-NH_2-mPEG NPs, and MnMEIO-silane-NH_2 NPs to Colo-205 cells (A). Binding activity of MnMEIO-silane-NH_2-(Erb)-mPEG NPs (B) or MnMEIO-silane-NH_2-(Erb) NPs (C) to A431, PC-3, and Colo-205 cells. In these experiments NPs (10 μg/ml) were incubated with cells at 37 °C for 1 h. Cell-associated fluorescent intensities were analyzed with a FACScan flow cytometer.

control probes (MnMEIO-silane-NH_2-(Erb) NPs, MnMEIO-silane-NH_2-mPEG NPs and MnMEIO-silane-NH_2 NPs) and cell-associated fluorescence were measured by a flow cytometer. As shown in Fig. 3 (A) minor MnMEIO-silane-NH_2-mPEG NPs and MnMEIO-silane-NH_2 NPs were found to bind the Colo-205 cells. In these cases, it is notable that MnMEIO-silane-NH_2-mPEG NPs showed lower nonspecific binding than MnMEIO-silane-NH_2 NPs, suggesting that PEG indeed masks the surface charges and reduces nonspecific binding of the NPs to cell membranes (Fig. 3 (A) and Supporting Information, Figures S14 and S15). On the contrary, as shown in Fig. 3 (B) and (C), slightly lower fluorescence was recorded in A431, PC-3, and Colo-205 tumor cells when treated with MnMEIO-silane-NH_2-(Erb)-mPEG NPs than that of treated with MnMEIO-silane-NH_2-(Erb) NPs. As Colo-205 tumor cells express little or none EGFR, both MnMEIO-silane-NH_2-(Erb)-mPEG NPs and MnMEIO-silane-NH_2-(Erb) NPs were expected to bind poorly to

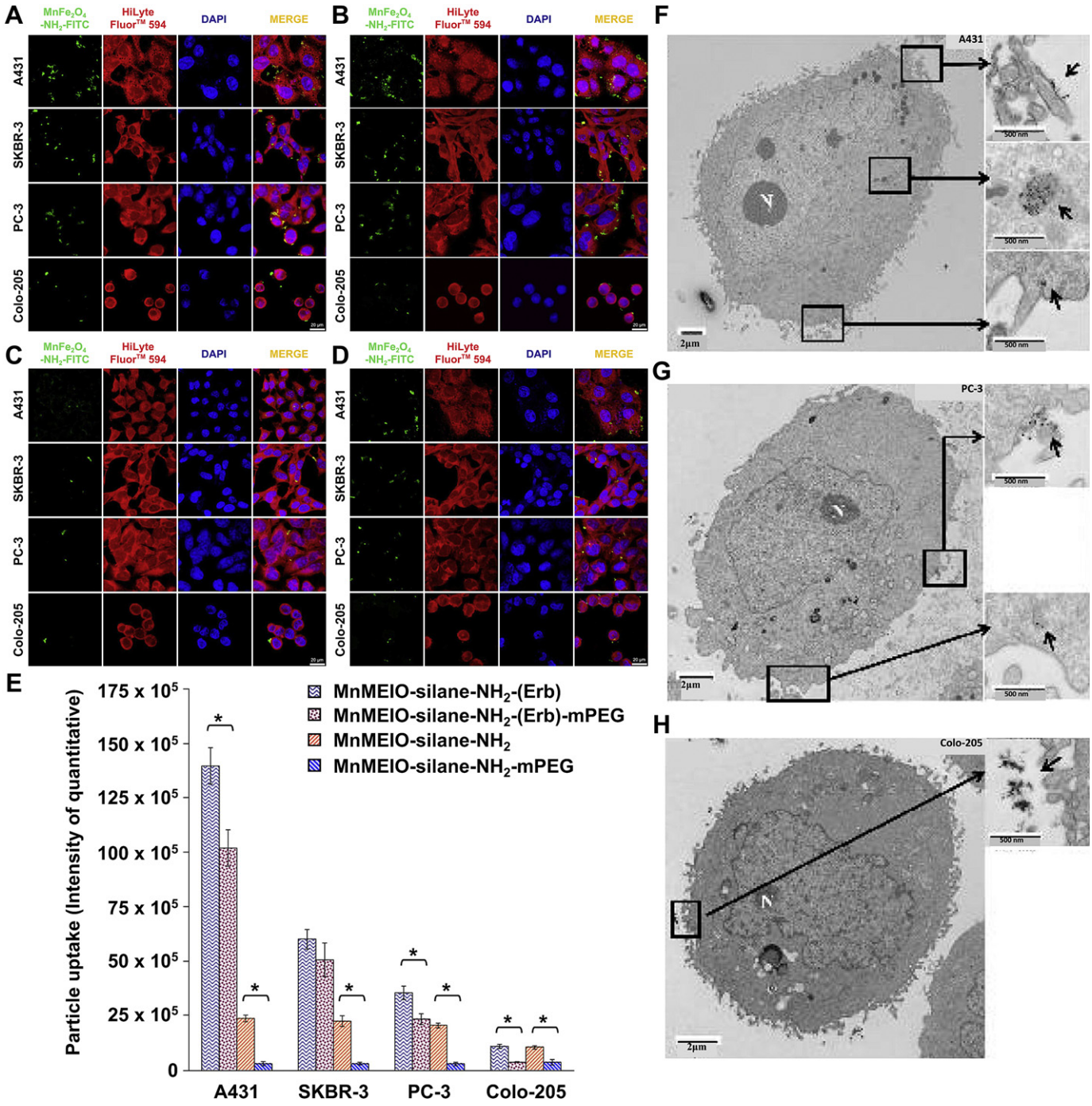

Fig. 4. Analyses of the specificity of the NPs. MnMEIO-silane-NH_2-(Erb)-mPEG (A), MnMEIO-silane-NH_2-(Erb) (B), MnMEIO-silane-NH_2-mPEG (C), and MnMEIO-silane-NH_2 NPs (D) were incubated (10 μg/mL) with cell lines at 37 °C for 1 h. Cells were counterstained for cytoplasm (with HiLyteFluor™ 594 in red) and nuclei (with DAPI in blue), then observed under a confocal microscopy using appropriate filters. In these NPs, FITC was conjugated in place of the Cy777 shown in Fig. 2. (E) Quantitative fluorescent intensities of the NPs in the tumor cells. Data are represented as mean ± SD. $n = 3$. $^*P < 0.05$. TEM analysis of the cellular uptake of MnMEIO-silane-NH_2-(Erb)-mPEG NPs (10 μg/mL) in A431 (F), PC-3 (G) and Colo-205 (H) cells. The black dots shown in insets are MnMEIO-silane-NH_2-(Erb)-mPEG NPs (short arrows). (For interpretation of the references to color in this figure legend, the reader is referred to the web version of this article.)

Colo-205 cells. However, MnMEIO-silane-NH_2-(Erb) NPs displayed more nonspecific binding to Colo-205 cells than that of MnMEIO-silane-NH_2-(Erb)-mPEG NPs. Exposed amine groups may generate positive charges on the surfaces of nanoparticles and positively charged nanoparticles are known to enhance adsorption to negatively charged cell membranes compared to neutral or negatively charged nanoparticles [14,16]. Since MnMEIO-silane-NH_2-(Erb) NPs and MnMEIO-silane-NH_2-(Erb)-mPEG NPs differ only at the position of the amine groups (which were used for conjugation with Erb (Fig. 2)), difference in nonspecific binding activities in these two probes is best explained by masking of surface charges by the terminal flexible mPEG arms.

3.3. Confocal fluorescence imaging

We used confocal microscopy to investigate the binding efficiency and specificity of the probes. In these experiments FITC was conjugated to the respective nanoparticles in place of Cy777 shown in Fig. 2. Consistent with the flow cytometric results, Erb on the nanoparticles can target EGFR efficiently; graded FITC fluorescent intensity was observed on the cell membranes of A431 cells, SKBR-3 and PC-3 cells, reflecting EGFR expression levels on the membranes in these cells (Fig. 4).

Although MnMEIO-silane-NH_2-(Erb) seemingly gave rise to stronger fluorescent signals than that of MnMEIO-silane-NH_2-(Erb)-mPEG, some of the signals were attributed to nonspecific binding as more MnMEIO-silane-NH_2-(Erb) bound to Colo-205 cells which express little or none EGFR. Higher magnification of confocal microscopy revealed that MnMEIO-silane-NH_2-(Erb)-mPEG NPs and MnMEIO-silane-NH_2-(Erb) NPs resided in the cytoplasm of tumor cells, suggesting the uptake of NPs by the EGFR-expressing tumor cells, possibly via receptor-mediated endocytosis. In contrast, in the absence of Erb antibodies the control probes (MnMEIO-silane-NH_2-mPEG and MnMEIO-silane-NH_2) did not differentially stain tumor cells according to their EGFR levels. In these experiments, however, MnMEIO-silane-NH_2-mPEG stained less than MnMEIO-silane-NH_2 in all the cells we tested, highlighting the effectiveness of our strategy of masking surface charges by a flexible mPEG arm to enhance imaging specificity. Thus, these data indicate that first, tumor-targeting moiety can direct the conjugated probes to the tumor cells and second, the flexible mPEG can mask positive charges on the surfaces of the probe to effectively reduce nonspecific binding to tumor cells.

3.4. TEM measurements

Similar finding was observed in TEM images of tumor cells (A431, PC-3, and Colo-205) incubated with MnMEIO-silane-NH_2-(Erb)-mPEG NPs. As shown in Fig. 4 (F), the nanoparticles (black dots) resided in the cytoplasm, suggesting that MnMEIO-silane-NH_2-(Erb)-mPEG NPs were trapped by the tumors possibly via receptor-mediated endocytosis. In addition, few black dots were revealed in PC-3 cells (Fig. 4 (G)), but were absent in Colo-205 cells (Fig. 4 (H)). These results clearly showed masking of surface charges can efficiently avoid nonspecific binding.

3.5. In vitro MR imaging

To test its usefulness for *in vitro* imaging, MnMEIO-silane-NH_2-(Erb)-mPEG was incubated with A431, PC-3, and Colo-205 tumor cells. Treated cells were followed by T_2-weighted *in vitro* MR imaging. Fig. 5 shows representative *in vitro* T_2-weighted images of tumor cells treated with or without MnMEIO-silane-NH_2-(Erb)-mPEG. The contrast enhancement (%) values for A431, PC-3, and Colo-205 tumor cells after MnMEIO-silane-NH_2-(Erb)-mPEG treatments were −97.1%, −49.7%, and −2.8%, respectively. A431 cells showed strongest enhancement comparing to PC-3 and Colo-205 cells. These *in vitro* MR images results indicate that MnMEIO-silane-NH_2-(Erb)-mPEG could efficiently target to EGFR-overexpressing tumor cells for MR imaging.

3.6. In vivo MR imaging

To test its utility for *in vivo* MR imaging, nude mice bearing subcutaneous A431 and Colo-205 tumor cells in right and left lateral thighs, respectively, were intravenously injected with MnMEIO-silane-NH_2-(Erb)-mPEG NPs, MnMEIO-silane-NH_2-(Erb) NPs, MnMEIO-silane-NH_2-mPEG NPs, and MnMEIO-silane-NH_2 NPs (10 mg/kg) and subjected to MR imaging. Consistent with our *in vitro* studies, highest imaging specificity was noted in mice treated with MnMEIO-silane-NH_2-(Erb)-mPEG probes. The relative contrast enhancements were 7.94 (−45.3% versus −5.7%, 2 h post-injection), and 7.59 (−62.3% versus −8.2%, 24 h post-injection) fold higher in A431 tumors as compared to the EGFR-negative Colo-205 tumors (Fig. 6). On the contrary, significant negative contrast enhancements were noted in Colo-205 tumors after injection of the MnMEIO-silane-NH_2-(Erb) NPs; the relative contrast enhancements were only 1.44 (−50.6% versus −35.1%, 2 h post-injection) and 1.52 (−68.7% versus −45.1%, 24 h post-injection) fold higher in A431 tumors as compared to the EGFR-negative Colo-205 tumors. Finally, MnMEIO-silane-NH_2-mPEG NPs and MnMEIO-silane-NH_2 NPs did not differentiate $EGFR^+$ or $EGFR^-$ tumors, and more nonspecific binding was noted in tumors after injection of MnMEIO-silane-NH_2 NPs.

3.7. In vivo optical imaging

MnMEIO-silane-NH_2-(Erb)-mPEG was designed as a dual-modality MR-optical imaging agent. Having established its utility

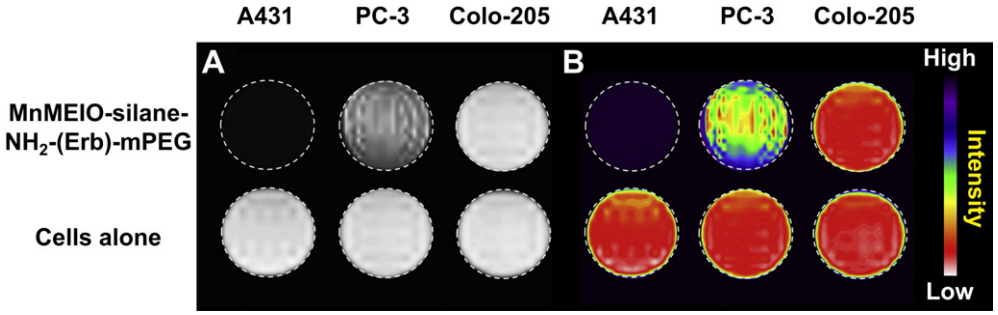

Fig. 5. EGFR-dependent contrast enhancement. (A) T_2-weighted MR images of EGFR-positive cell lines (A431 and PC-3 cells) and negative cell lines(Colo-205 cells) incubated with MnMEIO-silane-NH_2-(Erb)-mPEG NPs (10 μg/mL); (B) color-map of MR imaging.

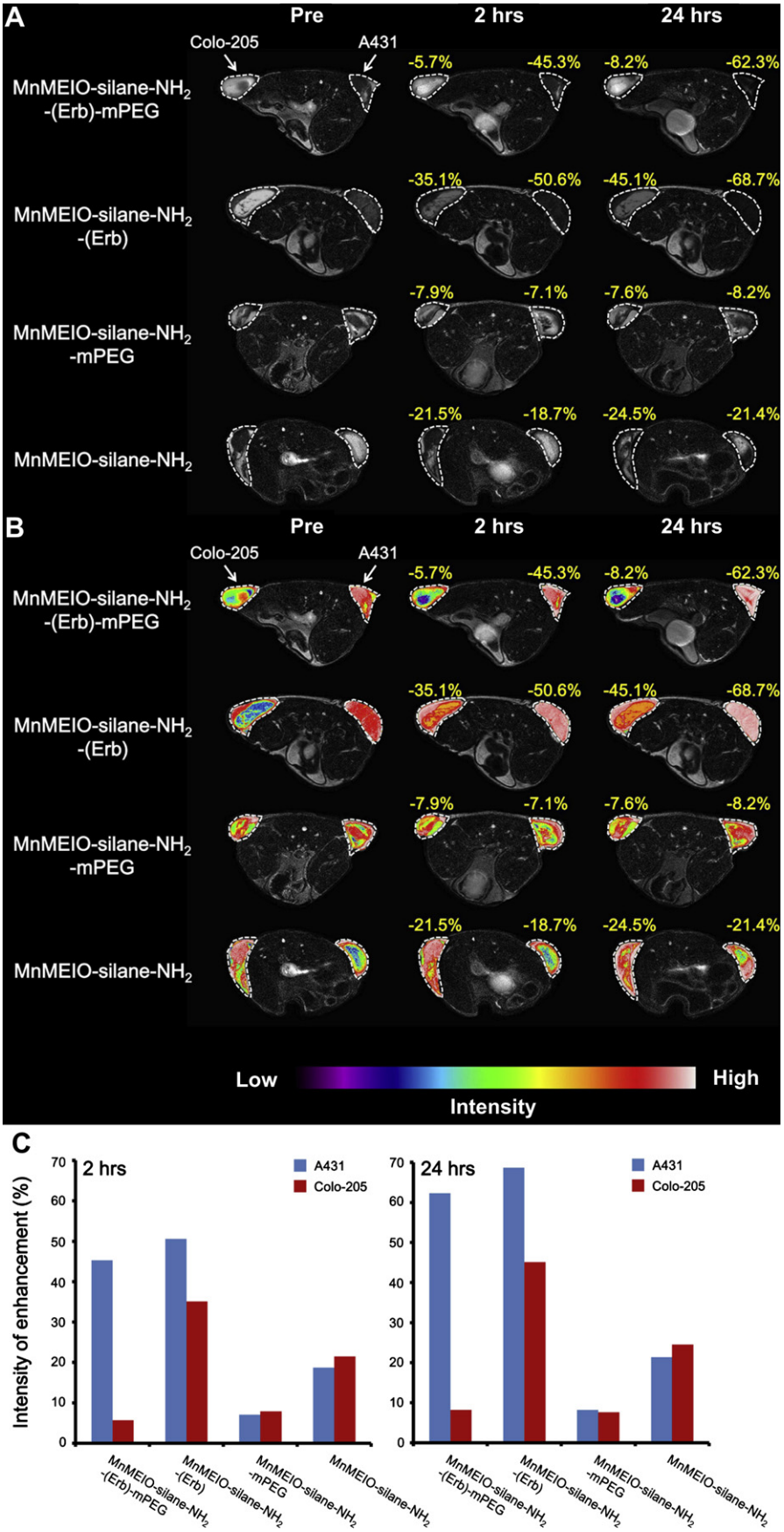

Fig. 6. (A) T_2-weighted MR images of nude mice bearing subcutaneous tumor xenografts of A431 and Colo-205 tumor cells before and after injection of MnMEIO-silane-NH_2-(Erb)-mPEG NPs and control probe (MnMEIO-silane-NH_2-mPEG NPs, MnMEIO-silane-NH_2-(Erb) NPs, and MnMEIO-silane-NH_2 NPs) (10 mg/kg). Images were acquired at pre-injection and various time points (2 and 24 h) post-injection; (B) Color-map of MR imaging; (C) Histograms of contrast enhancements in different tumors after injections of the probes.

in MR imaging, we further investigated whether it can be used in optical imaging. Nude mice bearing subcutaneous A431 and Colo-205 tumors were intravenously injected with MnMEIO-silane-NH_2-(Erb)-mPEG NPs, MnMEIO-silane-NH_2-(Erb) NPs, MnMEIO-silane-NH_2-mPEG NPs, and MnMEIO-silane-NH_2 NPs (10 mg/kg) (all of which bears an infrared dye Cy777, Fig. 2), and then subjected to whole-body optical imaging. Consistent with the *in vivo* MR imaging, highest imaging specificity was achieved when MnMEIO-silane-NH_2-(Erb)-mPEG was used (Fig. 7); fluorescent signal was evident in $EGFR^+$ A431 tumors but only very feeble in Colo-205 tumors at both 2 h and 24 h post-injection of the probe.

3.8. MnMEIO-silane-NH_2-mPEG as a base system for designing highly specific targeted imaging probes

MnMEIO-silane-NH_2-(Erb)-mPEG was generated by conjugating the EGFR targeting antibodies (Erb) to the reactive amine groups on the base probe, MnMEIO-silane-NH_2-mPEG. We demonstrated that the MnMEIO-silane-NH_2-(Erb)-mPEG NPs gave rise to highest imaging specificity by masking the positive charge of the probe. Furthermore, the base probe showed minimal nonspecific binding. Thus, we test our design strategy by replacing Erbitux with Herceptin, a HER2/neu-specific antibody to form a HER2/neu targeting imaging probe MnMEIO-silane-NH_2-(Her)-mPEG. As in the case of specific targeting of $EGFR^+$ tumors by MnMEIO-silane-NH_2-(Erb)-mPEG, the MnMEIO-silane-NH_2-(Her)-mPEG specifically targeted HER2/neu-expressing cells but not to non-expressing cells in confocal microscopy analyses and *in vitro* MR imaging. In addition, imaging intensity was proportional to their expression levels of HER2/neu (Supporting Information, Figure S16), indicating MnMEIO-silane-NH_2-(Her)-mPEG is a specific and efficient imaging probe for HER2/neu-expressing tumors. Conclusively, these data strongly support the notion that PEG can mask the positive charges on the imaging probes to enhance imaging specificity, and the internal configuration of amine group allows flexible choice of targeting antibodies yet preserves the benefit of masking effect by PEG.

3.9. Histological analysis and Immunostaining studies

The aforementioned interpretation is further supported by histological analysis (Supporting Information, Figure S17). Significant localization of MnMEIO-silane-NH_2-(Erb)-mPEG NPs was founded in A431 tumor biopsy. On the contrary, no uptake of MnMEIO-silane-NH_2-(Erb)-mPEG NPs was observed in Colo-205 tumor biopsy. These results clearly demonstrate that MnMEIO-silane-NH_2-(Erb)-mPEG NPs can very specifically target to EGFR-expressing sites *in vivo*.

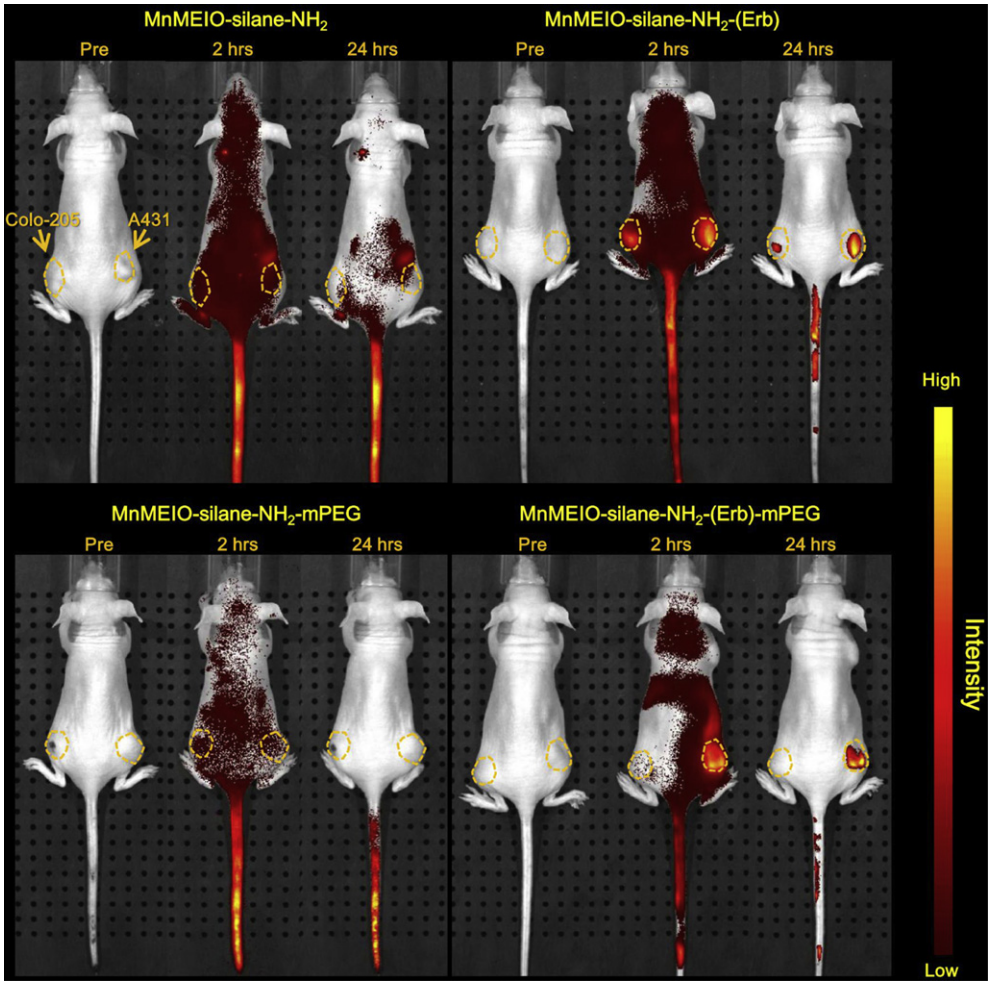

Fig. 7. *In vivo* optical images of nude mice bearing subcutaneous tumor xenografts of A431 and Colo-205 tumor cells after intravenous injection of MnMEIO-silane-NH_2-(Erb)-mPEG NPs and control probe (MnMEIO-silane-NH_2-mPEG NPs, MnMEIO-silane-NH_2-(Erb) NPs, and MnMEIO-silane-NH_2 NPs) (10 mg/kg). Images were acquired at pre-injection and various time points (2 h and 24 h) post-injection.

4. Conclusion

In summary, we have successfully developed a nanocarrier, MnMEIO-silane-NH_2-mPEG NPs, in which flexible mPEG arms was proposed to mask positive charges on the surface of the nanocarriers to prevent its nonspecific binding to cells. A unique dual-modality MR-optical imaging contrast agent, MnMEIO-silane-NH_2-(Erb)-mPEG was generated using MnMEIO-silane-NH_2-mPEG as backbone. Our data indicate positive charges generated by reactive amine groups ($-NH_2 \leftrightarrow NH_3^+$) on the surfaces of the nanocarriers are effectively masked by the flexible mPEG arms. We experimentally demonstrated that masking surface charges could significantly reduce nonspecific binding and increase the imaging specificity of MnMEIO-silane-NH_2-(Erb)-mPEG NPs to EGFR-overexpressing tumors *in vitro* and *in vivo*. Furthermore, the base probe can be conjugated with a variety of targeting antibodies yet preserve the benefit of masking effect by PEG. Based on these results, masking of the non-conjugated $-NH_2$ groups on nanocarriers is a promising strategy for the design and development of the next-generation nano-scale diagnostic and therapeutic modalities.

Acknowledgments

We are grateful to the National Science Council of the Republic of China for financial support under contracts no. NSC 100-2113-M-009-002 and NSC 100-2923-M-009-002-MYS. This research was also particularly supported by “Aim for the Top University Plan” of the National Chiao Tung University and Ministry of Education.

Appendix A. Supplementary data

Supplementary data related to this article can be found at http://dx.doi.org/10.1016/j.biomaterials.2013.02.025.

References

[1] Jennings LE, Long NJ. 'Two is better than one'-probes for dual-modality molecular imaging. Chem Commun 2009;24:3511–24.
[2] She H, Chen Y, Chen X, Zhang K, Wang Z, Peng DL. Structure, optical and magnetic properties of Ni@Au and Au@Ni nanoparticles synthesized via non-aqueous approaches. J Mater Chem 2012;22:2757–65.
[3] Yang L, Peng XH, Wang YA, Wang X, Cao Z, Ni C, et al. Receptor-targeted nanoparticles for *in vivo* imaging of breast cancer. Clin Cancer Res 2009;15:4722–32.
[4] Lee CM, Jang D, Kim J, Cheong SJ, Kim EM, Jeong MH, et al. Oleyl-chitosan nanoparticles based on a dual probe for optical/MR Imaging *in vivo*. Bioconjug Chem 2011;22:186–92.
[5] Foy SP, Manthe RL, Foy ST, Dimitrijevic S, Krishnamurthy N, Labhasetwar V. Optical imaging and magnetic field targeting of magnetic nanoparticles in tumors. ACS Nano 2010;4:5217–24.
[6] Liu F, Laurent S, Fattahi H, Vander Elst L, Müller RN. Superparamagnetic nanosystems based on iron oxide nanoparticles for biomedical imaging. Nanomed 2011;6:519–28.
[7] Hadjipanayis CG, Machaidze R, Kaluzova M, Wang L, Schuette AJ, Chen H, et al. EGFRvIII antibody-conjugated iron oxide nanoparticles for magnetic resonance imaging-guided convection-enhanced delivery and targeted therapy of glioblastoma. Cancer Res 2010;70:6303–12.
[8] Sun C, Du K, Fang C, Bhattarai N, Veiseh O, Kievit F, et al. PEG-mediated synthesis of highly dispersive multifunctional superparamagnetic nanoparticles: their physicochemical properties and function *in vivo*. ACS Nano 2010;4:2402–10.
[9] Veiseh O, Sun C, Gunn J, Kohler N, Gabikian P, Lee D, et al. Optical and MRI multifunctional nanoprobe for targeting gliomas. Nano Lett 2005;5:1003–8.
[10] Chen CL, Zhang H, Ye Q, Hsieh WY, Hitchens TK, Shen HH, et al. A new nano-sized iron oxide particle with high sensitivity for cellular magnetic resonance imaging. Mol Imaging Biol 2011;13:825–39.
[11] Salvador-Morales C, Zhang L, Langer R, Farokhzad OC. Immunocompatibility properties of lipid-polymer hybrid nanoparticles with heterogeneous surface functional groups. Biomaterials 2009;30:2231–40.
[12] Chen H, Wang L, Yeh J, Wu X, Cao Z, Wang YA, et al. Reducing non-specific binding and uptake of nanoparticles and improving cell targeting with an antifouling PEO-b-PgammaMPS copolymer coating. Biomaterials 2010;31:5397–407.
[13] Boutry S, Brunin S, Mahieu I, Laurent S, Vander Elst L, Müller RN. Magnetic labeling of non-phagocytic adherent cells with iron oxide nanoparticles: a comprehensive study. Contrast Media Mol Imaging 2008;3:223–32.
[14] Cao Z, Yu Q, Xue H, Cheng G, Jiang S. Nanoparticles for drug delivery prepared from amphiphilic PLGA zwitterionic block copolymers with sharp contrast in polarity between two blocks. Angew Chem Int Ed 2010;122:3859–64.
[15] Lin RY, Dayananda K, Chen TJ, Chen CY, Liu GC, Lin KL, et al. Targeted RGD-nanoparticles for high sensitive *in vivo* integrin receptor imaging. Contrast Media Mol Imaging 2012;7:7–18.
[16] Cho EC, Xie J, Wurm PA, Xia Y. Understanding the role of surface charges in cellular adsorption versus internalization by selectively removing gold nanoparticles on the cell surface with a I2/KI etchant. Nano Lett 2009;9:1080–4.
[17] Wang B, Zhang L, Bae SC, Granick S. Nanoparticle-induced surface reconstruction of phospholipid membranes. Proc Natl Acad Sci 2008;105:18171–5.
[18] Shieh DB, Cheng FY, Su CH, Yeh CS, Wu MT, Wu YN. Aqueous dispersions of magnetite nanoparticles with NH_3^+ surfaces for magnetic manipulations of biomolecules and MRI contrast agents. Biomaterials 2005;26:7183–91.
[19] Carpenter AW, Slomberg DL, Rao KS, Schoenfisch MH. Influence of scaffold size on bactericidal activity of nitric oxide-releasing silica nanoparticles. ACS Nano 2011;5:7235–44.
[20] Soonthornthum T, Arias-Pulido H, Joste N, Lomo L, Muller C, Rutledge T, et al. Epidermal growth factor receptor as a biomarker for cervical cancer. Ann Oncol 2011;22:2166–78.